The N-terminal amphipathic helix of Pex11p self-interacts to induce membrane remodelling during peroxisome fission

Su, Juanjuan; Thomas, Ann S; Grabietz, Tanja; Landgraf, Christiane; Volkmer, Rudolf; Marrink, Siewert; Williams, Chris; Melo, Manuel N

Published in:
Biochimica et biophysica acta

DOI:
10.1016/j.bbamem.2018.02.029

Publication date:
2018

BBA - Biomembranes 1860 (2018) 1292–1300

Contents lists available at ScienceDirect

BBA - Biomembranes

journal homepage: www.elsevier.com/locate/bbamem

The N-terminal amphipathic helix of Pex11p self-interacts to induce membrane remodelling during peroxisome fission

Juanjuan Su[a], Ann S. Thomas[b], Tanja Grabietz[b], Christiane Landgraf[c], Rudolf Volkmer[c,d], Siewert J. Marrink[a], Chris Williams[b], Manuel N. Melo[a,e,*]

[a] Molecular Dynamics, Groningen Biomolecular Sciences and Biotechnology Institute, University of Groningen, Nijenborgh 7, 9747AG Groningen, The Netherlands
[b] Molecular Cell Biology, Groningen Biomolecular Sciences and Biotechnology Institute, University of Groningen, Nijenborgh 7, 9747AG Groningen, The Netherlands
[c] Institut für Medizinische Immunologie, Charité-Universitätsmedizin Berlin, 10115 Berlin, Germany
[d] Leibniz-Institut für Molekulare Pharmakologie, 13125 Berlin, Germany
[e] Instituto de Tecnologia Química e Biológica António Xavier, Universidade Nova de Lisboa, Av. da República, 2780-157 Oeiras, Portugal

ARTICLE INFO

Keywords:
Peroxisome fission
Pex11
Aggregation
Membrane
Coarse-grain molecular dynamics

ABSTRACT

Pex11p plays a crucial role in peroxisome fission. Previously, it was shown that a conserved N-terminal amphipathic helix in Pex11p, termed Pex11-Amph, was necessary for peroxisomal fission *in vivo* while *in vitro* studies revealed that this region alone was sufficient to bring about tubulation of liposomes with a lipid consistency resembling the peroxisomal membrane. However, molecular details of how Pex11-Amph remodels the peroxisomal membrane remain unknown. Here we have combined *in silico*, *in vitro* and *in vivo* approaches to gain insights into the molecular mechanisms underlying Pex11-Amph activity. Using molecular dynamics simulations, we observe that Pex11-Amph peptides form linear aggregates on a model membrane. Furthermore, we identify mutations that disrupted this aggregation *in silico*, which also abolished the peptide's ability to remodel liposomes *in vitro*, establishing that Pex11p oligomerisation plays a direct role in membrane remodelling. *In vivo* studies revealed that these mutations resulted in a strong reduction in Pex11 protein levels, indicating that these residues are important for Pex11p function. Taken together, our data demonstrate the power of combining *in silico* techniques with experimental approaches to investigate the molecular mechanisms underlying Pex11p-dependent membrane remodelling.

1. Introduction

Peroxisomes are membrane-bound cellular organelles that are found in almost all eukaryotes. They perform various metabolic functions, including the β-oxidation of fatty acids and detoxification of reactive oxygen species, especially hydrogen peroxide [1]. Failure in peroxisome formation in human cells results in peroxisome biogenesis disorders such as conditions of the Zellweger spectrum [2].

Peroxisomes are remarkably diverse and can change dramatically in abundance, size and content in response to numerous cues. Peroxisome numbers are maintained predominantly by fission, a multistep process including peroxisomal membrane elongation, constriction and scission [3]. The Pex11 protein, one of the most abundant peroxisomal membrane proteins, acts directly in peroxisomal fission in plants, yeasts and mammals. It participates in early stages of the cascade by initiating elongation of the peroxisomal membrane prior to fission [4,5]. Following this, members of the dynamin-related protein1 (DRP1) family [6,7], together with Fis1p [8] and Pex11p [9], bring about the final fission step. DRPs belong to a superfamily of large GTPases that regulate membrane structure *via* oligomerization and GTP-dependent conformational changes [10,11]. DRPs can assemble to form helical structures *in vitro* [12] and are termed “mechanoenzymes” due to their ability to translate chemical energy into mechanical force [13]. They can be recruited to the required site of action by sensing areas of high membrane curvature [14]. Members of this family involved in peroxisome fission include Drp3A in *Arabidopsis thaliana* [15], Vps1p and Dnm1p in the yeast *Saccharomyces cerevisiae* [7], Dnm1p in the yeast *Hansenula polymorpha* and the fungi *Penicillium chrysogenum* [16,17], and Drp1 in mammals [6,18]. Fis1p is a tail anchored membrane protein that associates with membranes through its C-terminal transmembrane domain. Fis1p interacts with DRPs in yeasts and mammals [19,20] while it was also reported to bind Pex11p [21,22]. Fis1p contributes to fission by recruiting DRPs to organelles and it is also likely to play a role in DRP self-assembly [19,23,24].

* Corresponding author at: Molecular Dynamics, Groningen Biomolecular Sciences and Biotechnology Institute, University of Groningen, Nijenborgh 7, 9747AG Groningen, The Netherlands.
E-mail address: m.n.melo@itqb.unl.pt (M.N. Melo).

https://doi.org/10.1016/j.bbamem.2018.02.029
Received 23 October 2017; Received in revised form 7 February 2018; Accepted 27 February 2018
Available online 01 March 2018

Although the pivotal role of Pex11p in peroxisomal fission is well established, the molecular mechanisms underlying Pex11p-dependent membrane elongation are still not fully understood. Recently Opaliński et al. demonstrated that the N-terminus of *P. chrysogenum* Pex11p (*Pc*Pex11p) contains a conserved amphipathic helix, termed Pex11-Amph, which binds to membranes and alters the shape of liposomes, leading to tubulation. Through the use of mutants, the amphipathic properties of Pex11-Amph were found to be crucial for the function of Pex11p in peroxisome proliferation [4], data that support a model where Pex11-Amph inserts into the peroxisomal membrane to induce membrane curvature. However, details of how Pex11-Amph induces membrane remodelling remain unknown due to the limitations of experimental methods.

In this work, we have used Molecular Dynamics (MD) simulations to investigate the interplay between Pex11-Amph from *P. chrysogenum* [4] and a model peroxisomal membrane. We used the MARTINI coarse-grained (CG) force field [25], which enabled the use of large system sizes required to observe the collective peptide effect on membrane remodelling [26]. Our CG MD simulations revealed specific aggregation patterns of Pex11-Amph on the model membrane. With this information we were able to design loss-of-function mutant peptides that displayed decreased aggregation profiles *in silico*. Peptides bearing these mutations displayed a reduced ability to alter the morphology of liposomes *in vitro*, while we also demonstrate that these residues play an important role in Pex11p function *in vivo*. Taken together, this work illustrates the power of combining MD simulations with experiments to investigate the molecular mechanisms of membrane remodelling.

2. Materials and methods

2.1. Simulation setup

The lipid compositions of the membranes are the same as used by Opaliński et al. [4]. Three different lipid composition model membranes were built up: DOPC (1,2-dioleoyl-sn-glycero-3-phosphocholine), DOPC/DOPE (1,2-dioleoyl-sn-glycero-3-phosphoethanolamine) at a ratio of 70:30, and DOPC/DOPE/DOPS (1,2-dioleoyl-sn-glycero-3-phospho-L-serine)/CL (tetra oleoyl-cardiolipin)/PI (phosphatidylinositol) at a ratio of 55:30:5:5:5 - the last mixture mimicking the phospholipid composition of the peroxisomal membrane from the yeast *Pichia pastoris*. The simulated peptide is the *P.chrysogenum* Pex11-Amph, with sequence YNAVKKQFGTTRKIMRIGKFLEHLKAAA. The secondary structure was assumed to be entirely α-helical. Membrane patches of the composition described above, periodic in the *x* and *y* dimensions, were built using the *insane* tool [27]. The lipids were described by MARTINI lipid parameters [25,28–31]. For the peptides, the improved MARTINI protein parameters [32] were employed.

2.2. Peptide number and placement

The concentration of peptide in the membrane used in experiments is difficult to know exactly, since part of the peptide will remain in the aqueous phase and only a fraction will partition to the bilayers. Knowing the global concentrations of liposomes and peptides, and assuming a typical partition constant, K_p, of 10^4 for the binding of cationic alpha-helical peptides to anionic membranes [33], one can estimate the bound peptide fraction as: $X_L = \frac{K_p \gamma_L [L]}{1 + K_p \gamma_L [L]}$, in which [L] is the global phospholipid concentration and γ_L the lipids' molar volume as a bilayer (approximately $0.8\,M^{-1}$ for fluid bilayers) [33]. Using the experimental peptide and lipid concentration from Opaliński et al. [4], of 50 μM and 0.65 mg/ml, respectively, this estimate yielded a bound lipid-to-peptide ratio of 20:1 (lipid concentration conversion to molar units was performed using each of the components' exact molar mass — for DOPC, DOPE, DOPS and CL — or the average molar mass — for PI). The estimate also assumed that the bound ratio was the same for all lipid compositions, which is likely not the case (as zwitterionic membranes will have a weaker charge interaction with the peptides). Simulations at a constant bound ratio were chosen so as to highlight any composition-specific behaviour differences that might otherwise be masked by the use of different concentrations. On attempting to place peptides on a single leaflet at the 20:1 global lipid-to-peptide ratio we found the peptides become impractically crowded. We settled, then, for placing the peptides on a single leaflet at a 40:1 lipid-to-peptide ratio, which locally corresponds to the 20:1 ratio as long as the peptides remain bound to that leaflet.

To place the peptides on the membrane surface but allow time for an optimal orientation to be reached and prevent untimely aggregation the following procedure was developed: the peptides were distributed on a plane in a way to have the desired density without peptide–peptide contacts. This peptide surface was placed above an equilibrated membrane (at an average 2.5 nm distance between backbone beads and the centre of the bilayer) and solvent/lipid contacts were relaxed by a 2000-step steepest descents energy minimization procedure. An equilibration was then carried out to let the peptides rotate and find their most favourable interaction interface with the membrane, for at least 1 μs (although converged rotation could already be attained in the 500 ns scale). During this equilibration peptides were prevented from leaving the membrane by imposing a harmonic potential in *z* of 500 kJ/mol/nm on each peptide's N and C terminal backbone beads. To prevent lateral diffusion and premature peptide–peptide interactions, the same N and C terminal beads were restrained in *x* and *y* movement (with 200 kJ/mol/nm force) for the duration of this adsorption procedure. This set of terminal restraints allows the peptides to rotate around their helical axis, and therefore adopt the most favourable orientation to interact with the bilayer. This initial construction of the system was done at a small scale (~400 lipids and 11 peptides), that was then multiplied to the final size for production. Fig. 1 shows the models of lipids, peptides, and a snapshot of one of the membrane systems for production — which contain around 4000 lipids and 99 peptides, with an initial box size of 38 nm × 38 nm × 16 nm. These membrane systems were then production-run for at least 5.3 μs without any restraints.

2.3. Simulation parameters

All the MD simulations were performed using the GROMACS software package version 4.6 [34]. Periodic boundary conditions in all directions were imposed. The temperature was weakly coupled (coupling time 1.0 ps) to 323 K, using the Berendsen thermostat [35]. The pressure was coupled (coupling time of 1.0 ps and compressibility of 3.0×10^{-4}), using a semi-isotropic Berendsen barostat, in which the lateral and perpendicular pressures were coupled independently at 1 bar, corresponding to a tension-free state of the membrane. A time step of 20 fs was used. Non-bonded interactions were computed using the "common" set of MARTINI parameters [36], implying switching the Lennard-Jones potentials to zero from 0.9 to 1.2 nm (pair-list update frequency of once per 10 steps) and electrostatics calculated as Coulomb interactions shifted to zero from 0 nm to the same 1.2 nm cutoff.

2.4. MD analysis

Peptide aggregation was initially analysed by counting backbone–backbone contacts at a 0.6 nm distance cutoff. Two peptides are counted as being in contact whenever each contacts at least three backbone beads of the other. The peptides can then be divided into clusters, where a peptide contacts at least one peptide of the remaining cluster. For each peptide pair in contact a contact map can also be drawn up. We used the method described by Fraser et al. [37] to group the contact maps of all the peptide pairs, over the entire trajectory time, with the similarity metric of Jarvis et al. [38]. Since contact map analysis did not yield a clear aggregation mode, focus was then put on analysing the indiscriminate contact counts per residue. This was

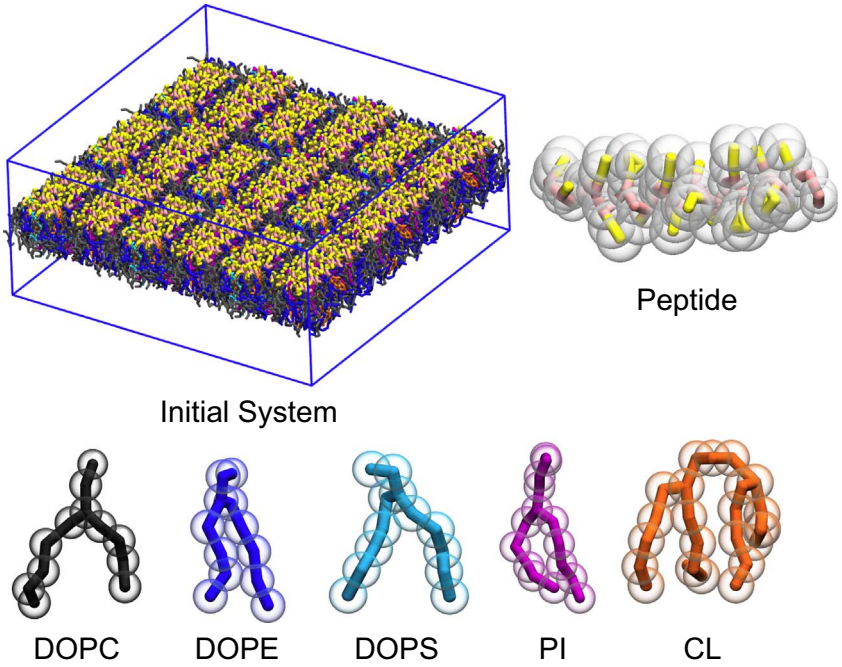

Fig. 1. Overview of simulation setup. Simulation box for the initial peptide + membrane system (solvent omitted for clarity; backbone of peptides in pink and side chains in yellow), together with a representation of the coarse-grain model for the peptide and lipids.

performed by tallying all neighbouring residues (within 1.0 nm) of each residue, regardless of the peptide contact status described above. Analyses were performed using in-house Python code, developed with extensive use of the MDAnalysis package [39,40].

2.5. Synthesis of peptides

The peptide arrays corresponding to the amino acids 56–83 of *Pc*Pex11p (WT) or *Pc*Pex11p bearing the point mutations Phe75, His78 and Leu79 to arginine (FHL-R) were synthesized on amino-modified cellulose membranes (β-alanine membrane) according to SPOT synthesis protocols [41]. The *e*-Pex11 and Pex11-Φ peptides are described in [4]. The sequences of the peptides used in this study are presented in Table S.1 of the supplementary material. Peptides were resuspended in lipid rehydration buffer (20 mM HEPES, 150 mM NaCl, pH 7.4) prior to use.

2.6. Preparation of SUVs

Small unilamellar vesicles (SUVs) were prepared according to [4] using chloroform solutions of DOPC, DOPE, DOPS, CL, and PI (natural mixture from bovine liver). Lipids were obtained from Avanti Polar Lipids. Liposomes were prepared by mixing the following concentrations of lipids together: DOPC 55 mol%, DOPE 30 mol%, DOPS 5 mol%, CL 5 mol%, PI 5 mol%. A nitrogen stream was used to evaporate the chloroform and the lipid film was stored in vacuum overnight. Following rehydration in lipid rehydration buffer (20 mM HEPES, 150 mM NaCl, pH 7.4), a final concentration of 0.8 mg/ml was obtained. SUVs of desired diameter were produced by extruding the liposomes through a polycarbonate filter (Avestin) with a pore size of 100 nm.

2.7. Peptide binding assay

SUVs and peptides were mixed to a final concentration of 0.65 mg/ml lipids and 50 μM peptides in a volume of 250 μl in lipid rehydration buffer. After incubating the mix for 20 min at room temperature, a sample of 50 μl was taken and pelleted by ultracentrifugation (21 °C, 20 min, 100 000 × *g*). The pellet was resuspended in 200 μl of lipid rehydration buffer. Equal volumes of the supernatant and pellet fraction were then subjected to a 16% Tricine-Gel along with a sample of the total fraction. Bands were visualized using silver staining (BioRad).

2.8. In vitro peptide-peptide interactions

Wild type (WT) and FHL-R mutant peptides (20, 5 and 1.25 pmoles) were subjected to native gel analysis using the NativePAGE™ system (Invitrogen). Due to the high pI values of the peptides (WT 10.6; FHL-R 11.8), gels were run with reversed polarity. Peptides on the gel were visualized using coomassie blue staining.

2.9. Turbimetric measurements

Measurements were performed as described in [4]. SUV solutions (0.4 mg/ml) were mixed with peptides (0 to 20 μM) in Lipid rehydration buffer. Absorbance was recorded at 400 nm for 1 min at room temperature using a Perkin Elmer Lambda 35 spectrophotometer. Changes in absorbance were plotted against peptide concentration.

2.10. Construction of plasmids and strains

Plasmids and oligonucleotides used in this study are listed in Tables S.2 and S.3 of the supplementary material, respectively. The plasmid pANN0016 bearing PcPex11-GFP along with the triple point mutations phenylalanine (75), histidine (78), leucine (79) to arginine was constructed as follows: a 628 bp DNA fragment, encoding for the N-terminal region of PcPex11p containing the point mutations, complete with *Hin*dIII and Eco47III restriction sites, was synthesized by the gBlock method (Integrated DNA Technologies). The fragment was digested with HindIII and Eco47III and ligated into HindIII-Eco47III digested PAMO-PcPex11-GFP plasmid (pLMO055 [4]) to generate the plasmid PAMO-PcPex11FHL-R-GFP (pANN016). Note that pANN016 was only used for cloning purposes in this study and was not introduced into *H. polymorpha* cells.

Plasmids for expression of the WT and mutant forms of *Pc*Pex11p, complete with Hemagglutinin (HA) tag, driven by the strong alcohol oxidase (*AOX*) promoter (to maximize protein production) were

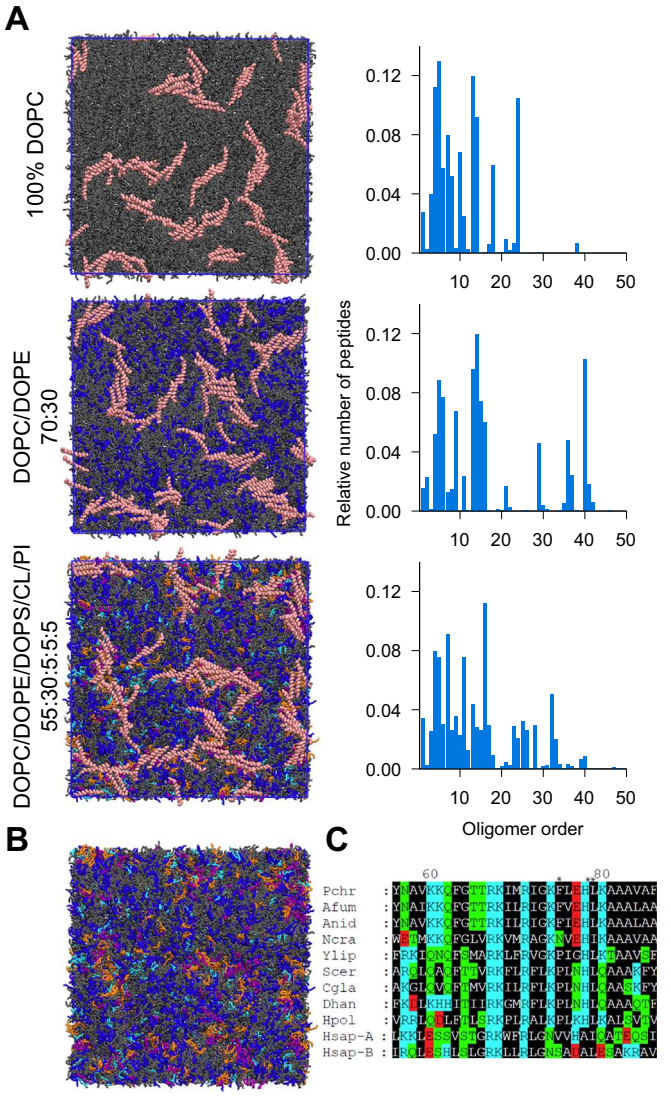

Fig. 2. A. Pex11-Amph peptides cluster on different membranes. Left panels are membrane top views after 2.7 μs; right panels represent the distribution of cluster size as the proportion of intervening peptides over the total number of peptides (*i.e.*, a single hexamer yields a bar twice as tall as a single trimer), averaged over the entire trajectory. Compositions are indicated for each system and lipids follow the same colouring scheme as in Fig. 1; backbones of peptide are shown in pink. B. Membrane top view of the same DOPC/DOPE/DOPS/CL/PI system as in A but with peptides hidden to reveal the underlying lipids (mostly cardiolipins). C. Sequence alignment of N-terminal amphipathic helix of Pex11 proteins from various species. Positively charged amino acids are conserved within the helix. Residues are coloured based on the physico-chemical properties of amino acids as follows: hydrophilic, charged: D, E (red), K, R, H (blue); hydrophilic, neutral: S, T, Q, N (green); hydrophobic: A, V, L, I, M, W, F, Y, G, P (black). The conserved helix consists of hydrophobic and polar, positively charged residues arranged in a recurrent manner. Abbreviations and accessions numbers used in sequence alignments: Pc: *Penicillium chrysogenum*, AAQ08763; Af: Aspergillus fumigatus, EAL88627; An: *Aspergillus nidulans*, EAA65086; Nc: *Neurospora crassa*, XP_960428; Yl: *Yarrowia lipolytica*, CAG81724; Sc: *Saccharomyces cerevisae*, CAA99168; Cg: *Candida glabrata*, Db: *Debaryomyces hansenii*, CAG84534; Hp: *Hansenula polymorpha*, DQ645582; HsA: *Homo sapiens* Pex11a, AAH09697; HsB: *Homo sapiens* Pex11b, AAH11963. Numbers denote amino acids positions in the alignment and asterisks denote residues that were mutated.

constructed as follows: a 763 bp fragment encoding *Pc*Pex11p WT or *Pc*Pex11p FHL-R along with a C-terminal HA tag was amplified from pLMO0055 or pANN0016 using primers ANN PR85 and ANN PR86. PCR products were digested with the enzymes *Hin*dIII and *Xba*I and ligated into HindIII-XbaI cut pHIPZ4-Nia [42] to obtain P*AOX*-*Pc*Pex11-HA (pANN0017) or P*AOX*-*Pc*Pex11FHL-R-HA (pANN0018) plasmids. *Nsi*I was used for linearization of the plasmid prior to transformation into *H. polymorpha pex11* cells bearing the peroxisomal marker PMP47-GFP [43]. All integrations were checked by colony PCR.

2.11. Strains and cultivation conditions

The *H. polymorpha* strains used in this study are listed in Table S.4 of the supplementary material. *H. polymorpha* cells were grown in batch cultures at 25 °C on mineral media [44] supplemented with 0.25% glucose or 0.5% methanol as carbon source and 0.25% ammonium sulphate or methylammonium chloride as nitrogen source. Leucine, when required, was added to a final concentration of 30 μg/ml. For growth on plates, YPD (1% yeast extract, 1% peptone and 1% glucose) media was supplemented with 2% agar. Resistant transformants were selected using 100 μg/ml zeocin or 100 μg/ml nourseothricin (Werner Bioagents). For cloning purposes, *Escherichia coli DH5a* was used as the host for propagation of plasmids. Cells were grown at 37 °C in Luria Bertani (LB) medium (1% Bacto tryptone, 0.5% Yeast Extract and 0.5% NaCl) supplemented with ampicillin (100 μg/ml). For growth on agar plates, 2% Agar was added to LB medium.

2.12. Biochemical techniques

Extracts prepared from cells treated with 12.5% trichloroacetic acid (TCA) were prepared for SDS-PAGE and Western blotting as detailed previously [45]. Equal amounts of proteins were loaded per lane. Blots were probed with mouse monoclonal antisera against the HA tag (H9658; Sigma-Aldrich) and rabbit polyclonal antisera against Pyc-1 (Loading control).

2.13. Fluorescence microscopy

All images were acquired at room temperature using a 100 × 1.30 NA Plan Neofluar objective. Wide-field images were taken using a Zeiss Axioscope A1 fluorescence microscope (Carl Zeiss, Sliedrecht, The Netherlands). Images were taken using a Coolsnap HQ2 digital camera and Micro Manager software. A 470/40 nm bandpass excitation filter, a 495 nm dichromatic mirror and a 525/50 nm bandpass emission filter was used to visualize the GFP signal. The levels of brightfield images were modified in such a way that only the circumference of the cell was visible. This image was subsequently changed in a blue colour to show the cell outline. For quantification of peroxisome numbers, strains were grown in duplicates and at least 100 cells were counted per strain. The number of peroxisomes in cells, made visible by the peroxisomal marker PMP47-GFP, was quantified manually. Significant differences between the groups were determined with a two-tailed unpaired *t*-test (https://www.graphpad.com/quickcalcs/ttest1/). The data represent the mean ± standard error of mean (SEM) of two biological replicates. For significance, p values < 0.05 are considered significant while p values < 0.01 are considered highly significant.

3. Results and discussion

3.1. In silico analysis

Pex11-Amph peptides were added onto three membrane systems: two model membranes composed of either pure DOPC or a DOPC/DOPE mixture, and an anionic DOPC/DOPE/DOPS/CL/PI membrane that mimics the lipid composition of peroxisomal membranes [4]. The initial system configuration is the one depicted in Fig. 1 — or analogous in the cases of the DOPC or DOPC/DOPE mixtures. Before the production runs the peptide orientations relative to the membrane were suitably relaxed by following a specific procedure that prevents free lateral diffusion and premature peptide–peptide interactions (see the Materials and Methods). Snapshots obtained after 2.7 μs simulation, together with the cluster size distributions of the peptides for the entire trajectories are shown in Fig. 2–A. We find that the Pex11-Amph

peptides aggregated on each of the three membrane systems. In all cases, aggregates formed, in a roughly linear fashion. Besides a slightly longer aggregate in the case of the charged membrane, there were no major differences in the aggregation behaviour between the three systems. The aggregation patterns were found to be quite stable at the timescale of the simulation, and once the peptides contacted each other they typically remained bound. Peptides remained mostly at the surface level, but more crowded aggregates caused some peptides to bulge out into the aqueous phase. This bulging away from the membrane surface occurred less in the charged membrane than in the other systems, presumably due to the more favourable electrostatic interactions between the cationic peptides and the anionic membrane (see Fig. S.1 in the Supplementary material). If taken to represent membrane affinity, this observation is consistent with the experimental work by Opaliński et al., in which the Pex11-Amph peptide was observed to bind the anionic liposomes most efficiently [4]. In addition to a putative higher affinity, we also observed that the anionic lipids that compose the charged membrane tend to cluster around the peptide aggregates (Fig. 2-B), which has been observed earlier in simulation studies [46]. Again, this is likely a consequence of the peptide–lipid electrostatic interactions, with potential relevance for the Pex11-Amph mechanism of action. Multiple sequence alignment of the amphipathic helix from different species revealed that a number of positive charges in this region are highly conserved among species (Fig. 2-C), suggesting their involvement in a conserved biological function. Given the similar behaviour of the peptide with the different membrane systems it was decided to proceed only with the charged membrane, which is also the most faithful peroxisome membrane mimetic.

The apparently regular peptide organization in the aggregates prompted a contact analysis to determine whether a preferred peptide–peptide binding pattern exists. Contact maps were obtained for all the peptide pairs, over the entire trajectory, and then clustered by similarity. However, peptide pair binding modes proved to be quite diverse, with no clear main aggregation pattern (data not shown). The peptides do bind preferably in a parallel fashion, although at several shifts relative to one another. A less discriminating approach was then chosen, in which the count of neighbouring residues was tallied for each residue (Fig. 3-A). The C-terminal half of the peptide is most involved in self-interaction. The anionic C terminus itself established the most contacts, predominantly with the cationic residues of neighbouring peptides, while residues Phe75, His78 and Leu79 were the most involved in sidechain–sidechain contacts. Interestingly, two of these residues are apolar, suggesting that it is not only charged interactions that rule aggregation.

To gauge the relevance of the binding residues Phe75, His78 and Leu79 in the aggregation process we mutated these residues to either aspartate (FHL-D) or arginine (FHL-R) residues. Runs were also carried out with the C-terminal charge removed — to understand its effect on aggregation but also to be closer to the physiological case where this peptide, being part of a larger protein, has no negative charge at that particular position. The snapshots for peptides after at least 2 μs simulations, and the respective aggregation size analysis are shown in Fig. 3-B. The C-terminus uncharged peptide is able to form linear structures, albeit with a higher number of monomers or low-order aggregates than Pex11-Amph. Nevertheless, the range of aggregation sizes still overlaps with that of the Pex11-Amph peptide. The aspartate mutant displays a strong aggregation profile, but clearly with a different and less ordered aggregation topology than the linear trains. This increase in self-interaction is likely due to the introduction of three anionic charges in a peptide that already has 8 cationic charges. In contrast, mutating the three residues to arginines abolished the linear pattern of aggregation, with the aggregation sizes becoming much smaller — mostly trimers and dimers. This highlights that the aggregation behaviour of Pex11-Amph results from a delicate balance between electrostatic attraction/repulsion and apolar interactions.

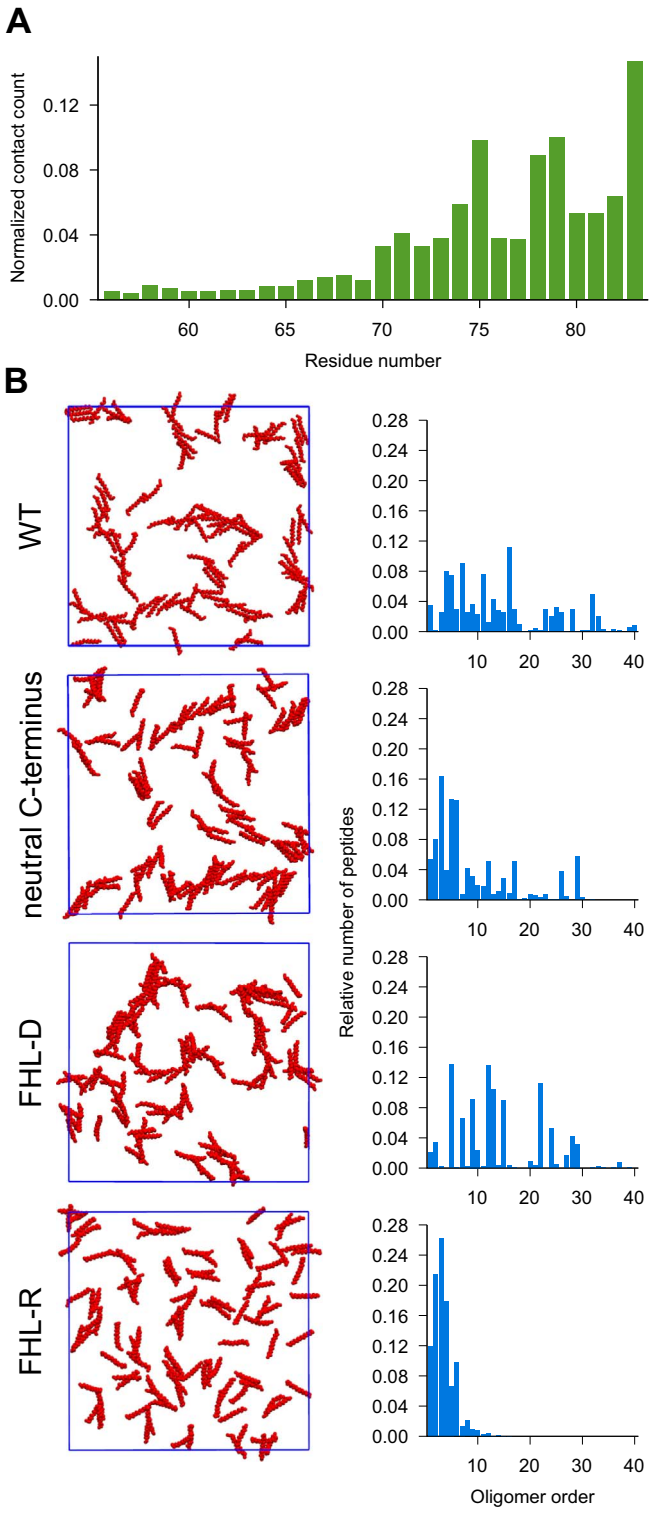

Fig. 3. A. Contact count of residues with residues of neighbouring peptides, for the Pex11-Amph peptide aggregates on a DOPC/DOPE/DOPS/CL/PI membrane. Besides the anionic C-terminus, residues Phe75, His78 and Leu79 establish the most peptide–peptide contacts. B. Aggregation behaviour of Pex11-Amph (labelled "wt") and different mutants (see text), on DOPC/DOPE/DOPS/CL/PI membranes. Left panels are top-view snapshots; right panels represent histograms of oligomer size distribution as in Fig. 2-B.

3.2. *In vitro analysis*

Having demonstrated that mutating residues Phe75, His78 and Leu79 to arginines impact on the ability of the Pex11 peptide to

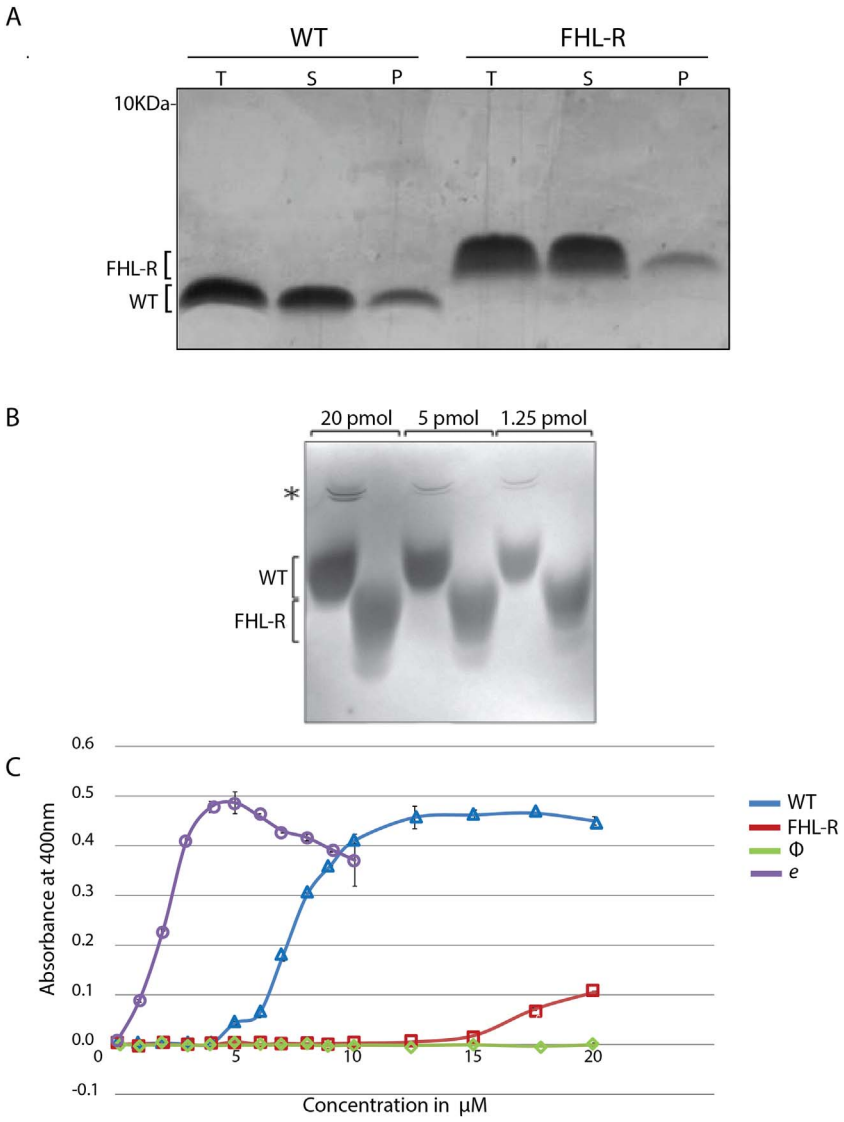

Fig. 4. Pex11-FHL-R mutant peptides can associate with liposomes but are impaired in their ability to alter liposome morphology. A. Binding of WT or FHL-R mutant peptides to liposomes: after incubation of peptides with liposomes followed by ultracentrifugation, 15 μl of the total (T; whole material before centrifugation), supernatant (S) and pellet (P) fractions were subjected to Tricine SDS-PAGE and visualized using silver staining. B. Native gel electrophoresis to investigate peptide-peptide interaction between WT or FHL-R mutant peptides. Bands became visible after coomassie blue staining of the gel. The asterisk indicates higher oligomeric isoforms of the WT peptide. C. Turbimetric analysis of liposomes after addition of increasing concentrations of WT (blue), FHL-R (red), *e*-Pex11 (purple) or Pex11-Φ (green) peptides. Increase in absorbance at OD 400 nm corresponded to increase in turbidity.

aggregate *in silico*, we next wanted to assess the behaviour of the Pex11 FHL-R peptide *in vitro*. First, we determined whether introducing the identified mutations affected the ability of the peptide to bind liposomes with a content mimicking the peroxisomal membrane. This was assessed through the presence of peptide in pelleted liposomes (P in Fig. 4-A). Similar to WT Pex11-Amph, the FHL-R mutant peptide was able to bind liposomes, albeit at a somewhat decreased level (Fig. 4-A). The replacement of apolar residues with the cationic arginine perhaps slightly compromises the capacity of the peptide to bind liposomes, since hydrophobic interactions are disturbed. Alternatively, a reduced affinity of the mutant peptide for liposomes could be a consequence of an excessive cationic density, beyond the ability of the peptide to cluster anionic lipids as observed for WT (Fig. 2-B). Nevertheless, our data indicate that the FHL-R peptide can associate with liposomes.

Next, we investigated whether WT and FHL-R peptides were able to form oligomers using native gel electrophoresis. Fig. 4-B shows that a small amount of the WT peptide could form higher oligomeric structures, as determined by the presence of higher bands in the native gel displayed in Fig. 4-B. This was not observed with the FHL-R peptide. Thus, we conclude that Phe75, His78 and Leu79 in Pex11-Amph are crucial for self-interaction. As demonstrated for several cellular processes, such interactions are essential to induce disturbances in the lipid bilayer [47–50], thereby allowing distension of the membrane prior to an event such as fission.

In order to analyse if aggregation of peptides on the membrane corresponded to their ability to alter the morphology of liposomes, turbidity assays were conducted. The ability of the Pex11-Amph to deform liposomes resembling the peroxisome membrane was previously tested using such assays [4]. These experiments use increased turbidity as a measure of morphological change in liposomes upon addition of a peptide. We conducted similar turbidity assays using both WT as well as the FHL-R mutant peptide to compare their ability to induce turbidity. A dramatic difference was recorded between the peptides. While the WT peptide could induce turbidity at low concentrations of peptide (~5 μM) and reached maximum activity at around 12.5 μM, the FHL-R mutant peptide elicited a response only when much higher concentrations of peptide were used (Fig. 4-C). Modified Pex11-Amph peptides that are known to cause extensive tubulation (*e*-Pex11) or a complete loss of function (Pex11-Φ) were used as positive or negative controls, respectively. Two residues were changed to tryptophans in *e*-Pex11 (I69W and A83W), so that the hydrophobic interface of the helix would become bulkier and better interact with the membrane, whereas Pex11-Φ contained mutations (I69E, I72E and F75E) that reduced binding to the hydrophobic surface [4]. Taken together, this experiment demonstrates that the FHL-R mutant peptide is severely affected in altering liposome morphology.

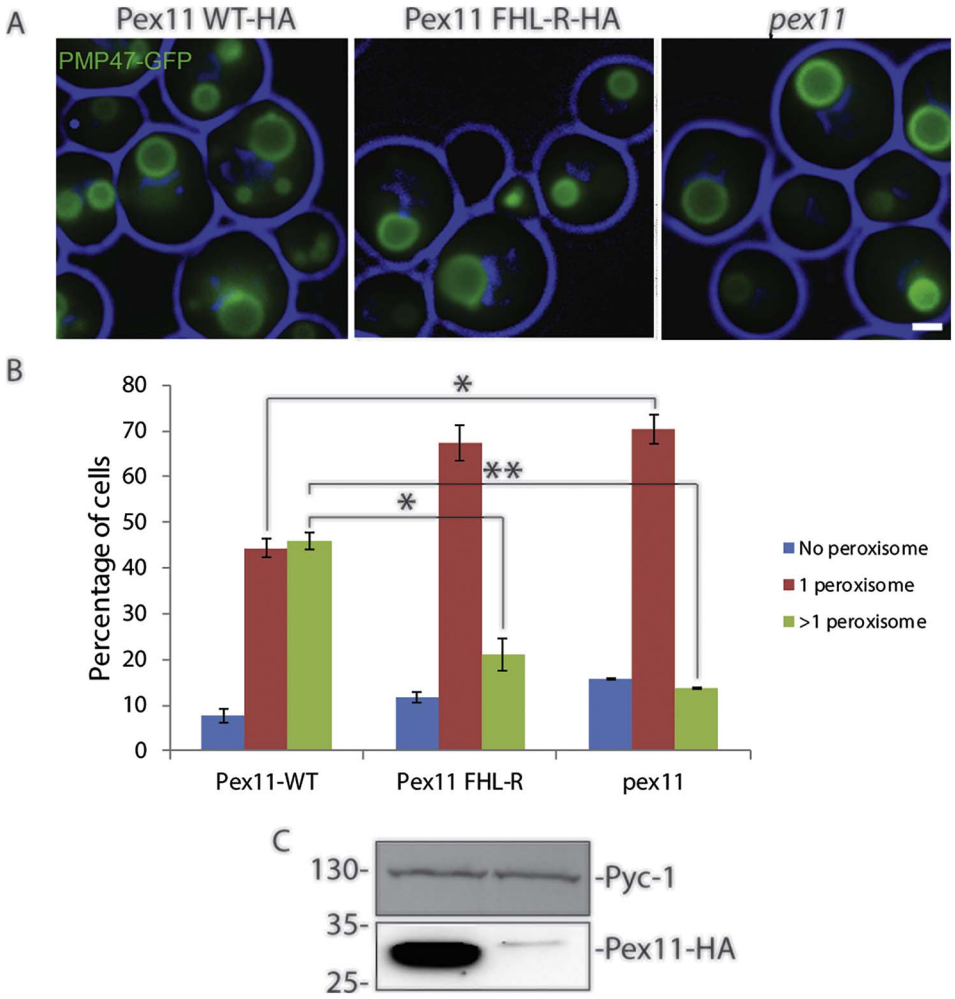

Fig. 5. Mutations to residues Phe75, His78 and Leu79 in *Pc*Pex11p destabilise the protein. A. *Hp pex11* cells bearing either WT or FHL-R mutant *Pc*Pex11p were grown for 60 h on methanol containing medium and visualized with fluorescence microscopy. The peroxisomal membrane protein PMP47 fused to GFP was used to mark peroxisomes. The blue colour represents the circumference of the cell (see materials and methods for details). Scale bar represents 1 μm. B. Quantification of peroxisome numbers from images represented in (A). For each experiment, at least 100 cells were counted per strain. Error bars represent the SEM between two separate experiments. * $p < 0.05$, ** $p < 0.005$. C. SDS-PAGE and western blot analysis of *Hp pex11* cells bearing WT or FHL-R mutant forms of HA-tagged *Pc*Pex11p probed with antibodies against the HA tag and Pyc-1 (loading control).

3.3. In vivo analysis

It has been reported that the production of the WT version of *Pc*Pex11p in *H. polymorpha* cells deleted for PEX11 (*Hp pex11*) stimulates the proliferation of peroxisomes [51]. To further validate our *in silico* and *in vitro* data and characterize the effect of these mutations on protein function *in vivo*, we constructed both a WT and a mutant version of *Pc*Pex11p bearing arginine mutations at positions Phe75, His78 and Leu79, complete with C-terminal HA tag, for expression in *H. polymorpha pex11* cells. The *H. polymorpha pex11* strain also produced the peroxisomal membrane protein PMP47 fused to GFP, to allow the analysis of peroxisome abundance by fluorescence microscopy. Quantification of fluorescence microscopy data performed on *pex11* cells bearing *Pc*Pex11p WT revealed an increase in peroxisome numbers relative to the *pex11* control (Fig. 5-A and B), which was not observed in the strain producing the mutant variant. However, western blot analysis indicated that the mutant protein was present in extremely low amounts (Fig. 5-C), suggesting that mutations to the residues Phe75, His78 and Leu79 in Pex11p have a destabilizing effect on the protein. It is possible that mutation of these residues interferes with hydrophobic interactions that are necessary to stabilize the protein on the peroxisomal membrane or perhaps these mutations inhibit the targeting of Pex11p to peroxisomes. Both scenarios could lead to protein destabilization and subsequently, protein degradation. While these data do not allow us to conclude that mutating Phe75, His78 and Leu79 in Pex11p specifically inhibits peroxisomal fission *in vivo*, they do indicate that these residues are crucial for Pex11p function *in vivo*.

4. Concluding remarks

Pex11 proteins are responsible for the maintenance of peroxisome populations in plants, yeasts and mammals [52–54]. Understanding Pex11p function in detail becomes relevant in the light of disorders that arise in the absence of this protein [55]. In this work, coarse-grain MD simulations were employed to gain insight into the membrane tubulating activity of Pex11-Amph at the molecular-level. Furthermore, this study establishes a number of MD simulation protocols for minimal bias approaches to simulating high densities of peptides on membranes.

While Pex11p has been implicated in the initial steps of the fission process, how it achieves this is not fully understood. Our MD simulations demonstrate that Pex11-Amph can form oligomers on the peroxisomal membrane while further simulations allowed us to design a non-oligomerizing mutant form of Pex11-Amph. Our *in vitro* data demonstrate that this mutant peptide indeed displays a loss of function, establishing a clear link between Pex11-Amph oligomerization and membrane remodelling. Support for a role for Pex11p oligomerization in peroxisomal fission can be found in several reports. Human Pex11pβ has been shown to oligomerize *via* an N-terminal amphipathic helix and this interaction was indispensable for membrane curvature [56]. In an independent study, Pex11pβ oligomerization was reported to form patches on the peroxisomal membrane, marking sites for the assembly of the fission machinery, while disturbing Pex11pβ oligomerization resulted in a block in peroxisomal fission [22]. Accumulation of Pex11p on the peroxisomal membrane was also observed in *H. polymorpha* cells lacking *DNM1*, with Pex11p concentrated at the base of a peroxisomal tubule extending into the bud [57]. Additionally, Pex11p in *S. cerevisiae*

is also known to interact with itself [58,59]. Taken together, our data fit a model where Pex11p oligomerization acts as the starting point for peroxisomal fission, which in turn facilitates remodelling of the peroxisomal membrane. Subsequently, additional components of the fission machinery, including Fis1p and DRP family members, are then recruited to the sites of membrane curvature, allowing the final scission step to take place.

The peroxisome membrane contains lipids such as phosphatidylcholine, phosphatidylethanolamine, phosphatidylserine, cardiolipin and phosphatidylinositol [60]. Cardiolipin is well known for its contribution to membrane bending and it has an important role in mitochondrial fission process [61,62]. Cardiolipin is a dimeric phospholipid with a small acidic head group and four acyl chains, which gives it a conical structure. Due to this property, cardiolipin has been classified as a “high curvature lipid”, since it exerts lateral pressure in a membrane consisting of other phospholipids, promoting membrane curvature. Our simulations further hint that Pex11-Amph interactions may result in the clustering of anionic lipids, such as cardiolipin, on the peroxisomal membrane (Fig. 2-B). A recent study showed that peroxisome numbers were unaffected in a strain in which cardiolipin synthesis was blocked [63]. However, it is possible that other negatively charged lipids such as phosphatidylserine take over the function of cardiolipin on the peroxisomal membrane under such conditions. Our data suggest that Pex11p may act in cohesion with negatively charged lipids, a suggestion that is supported by the large number of well conserved positively charged residues in Pex11p family members (Fig. 2-C).

In conclusion, our work provides the first detailed molecular insights into the membrane remodelling activity of Pex11p and illustrates the power of combining computer simulations with *in vivo* and *in vitro* experimental validation.

Author contributions

J.S., A.S.T., S.J.M., C.W. and M.N.M. designed the study, J.S. and M.N.M. performed molecular dynamics simulations, A.S.T. performed strain construction and *in vivo* analysis, A.S.T., T.G. and C.W. performed *in vitro* assays, C.L. and R.V. synthesized peptides, S.J.M., C.W. and M.N.M. supervised the project, J.S., A.T., S.J.M., C.W. and M.N.M. wrote the paper.

Transparency document

The http://dx.doi.org/10.1016/j.bbamem.2018.02.025 associated with this article can be found, in online version.

Acknowledgements

J.S. is supported by China Scholarship Council, A.S.T. is supported by the Erasmus-Mundus Svagata programme, C.W. is supported by a VIDI (723.013.004) grant and M.N.M. is supported by a VENI (722.013.010) grant from the Netherlands Organization for Scientific Research (NWO). M.N.M. is further supported by Project LISBOA-01-0145-FEDER-007660 (Microbiologia Molecular, Estrutural e Celular) funded by FEDER funds through COMPETE2020 - Programa Operacional Competitividade e Internacionalização (POCI) and by national funds through FCT - Fundação para a Ciência e a Tecnologia. The authors declare no conflict of interest.

Appendix A. Supplementary data

Supplementary data to this article can be found online at https://doi.org/10.1016/j.bbamem.2018.02.029.

References

[1] N.A. Bonekamp, A. Volkl, H.D. Fahimi, M. Schrader, Reactive oxygen species and peroxisomes: struggling for balance, Biofactors 35 (2009) 346–355.
[2] S.J. Steinberg, G. Dodt, G.V. Raymond, N.E. Braverman, A.B. Moser, H.W. Moser, Peroxisome biogenesis disorders, Biochim. Biophys. Acta 1763 (2006) 1733–1748.
[3] A. Koch, G. Schneider, G.H. Luers, M. Schrader, Peroxisome elongation and constriction but not fission can occur independently of dynamin-like protein 1, J. Cell Sci. 117 (2004) 3995–4006.
[4] L. Opalinski, J.A. Kiel, C. Williams, M. Veenhuis, I.J. van der Klei, Membrane curvature during peroxisome fission requires Pex11, EMBO J. 30 (2010) 5–16.
[5] J. Koch, K. Pranjic, A. Huber, A. Ellinger, A. Hartig, F. Kragler, C. Brocard, PEX11 family members are membrane elongation factors that coordinate peroxisome proliferation and maintenance, J. Cell Sci. 123 (2010) 3389–3400.
[6] A. Koch, M. Thiemann, M. Grabenbauer, Y. Yoon, M.A. McNiven, M. Schrader, Dynamin-like protein 1 is involved in peroxisomal fission, J. Biol. Chem. 278 (2003) 8597–8605.
[7] K. Kuravi, S. Nagotu, A.M. Krikken, K. Sjollema, M. Deckers, R. Erdmann, M. Veenhuis, I.J. van der Klei, Dynamin-related proteins Vps1p and Dnm1p control peroxisome abundance in Saccharomyces cerevisiae, J. Cell Sci. 119 (2006) 3994–4001.
[8] A.M. Motley, G.P. Ward, E.H. Hettema, Dnm1p-dependent peroxisome fission requires Caf4p, Mdv1p and Fis1p, J. Cell Sci. 121 (2008) 1633–1640.
[9] C. Williams, L. Opalinski, C. Landgraf, J. Costello, M. Schrader, A.M. Krikken, K. Knoops, A.M. Kram, R. Volkmer, I.J. van der Klei, The membrane remodeling protein Pex11p activates the GTPase Dnm1p during peroxisomal fission, Proc. Natl. Acad. Sci. U. S. A. 112 (2015) 6377–6382.
[10] J.A. Mears, L.L. Lackner, S. Fang, E. Ingerman, J. Nunnari, J.E. Hinshaw, Conformational changes in Dnm1 support a contractile mechanism for mitochondrial fission, Nat. Struct. Mol. Biol. 18 (2011) 20–26.
[11] D. Danino, K.H. Moon, J.E. Hinshaw, Rapid constriction of lipid bilayers by the mechanochemical enzyme dynamin, J. Struct. Biol. 147 (2004) 259–267.
[12] M.G. Ford, S. Jenni, J. Nunnari, The crystal structure of dynamin, Nature 477 (2011) 561–566.
[13] M.H. Stowell, B. Marks, P. Wigge, H.T. McMahon, Nucleotide-dependent conformational changes in dynamin: evidence for a mechanochemical molecular spring, Nat. Cell Biol. 1 (1999) 27–32.
[14] J.B. Fournier, P.G. Dommersnes, P. Galatola, Dynamin recruitment by clathrin coats: a physical step? C. R. Biol. 326 (2003) 467–476.
[15] S. Mano, C. Nakamori, M. Kondo, M. Hayashi, M. Nishimura, An Arabidopsis dynamin-related protein, DRP3A, controls both peroxisomal and mitochondrial division, Plant J. 38 (2004) 487–498.
[16] S. Nagotu, R. Saraya, M. Otzen, M. Veenhuis, I.J. van der Klei, Peroxisome proliferation in Hansenula polymorpha requires Dnm1p which mediates fission but not de novo formation, Biochim. Biophys. Acta 1783 (2008) 760–769.
[17] W.H. Meijer, L. Gidijala, S. Fekken, J.A. Kiel, M.A. van den Berg, R. Lascaris, R.A. Bovenberg, I.J. van der Klei, Peroxisomes are required for efficient penicillin biosynthesis in Penicillium chrysogenum, Appl. Environ. Microbiol. 76 (2010) 5702–5709.
[18] S. Gould, X. Li, The dynamin-like GTPase DLP1 is essential for peroxisome division and is recruited to peroxisomes in part by PEX11, J. Biol. Chem. 278 (2003) 17012–17020.
[19] Y. Yoon, E.W. Krueger, B.J. Oswald, M.A. McNiven, The mitochondrial protein hFis1 regulates mitochondrial fission in mammalian cells through an interaction with the dynamin-like protein DLP1, Mol. Cell. Biol. 23 (2003) 5409–5420.
[20] R.C. Wells, L.K. Picton, S.C. Williams, F.J. Tan, R.B. Hill, Direct binding of the dynamin-like GTPase, Dnm1, to mitochondrial dynamics protein Fis1 is negatively regulated by the Fis1 N-terminal arm, J. Biol. Chem. 282 (2007) 33769–33775.
[21] S. Joshi, G. Agrawal, S. Subramani, Phosphorylation-dependent Pex11p and Fis1p interaction regulates peroxisome division, Mol. Biol. Cell 23 (2012) 1307–1315.
[22] S. Kobayashi, A. Tanaka, Y. Fujiki, Fis1, DLP1, and Pex11p coordinately regulate peroxisome morphogenesis, Exp. Cell Res. 313 (2007) 1675–1686.
[23] A.D. Mozdy, J.M. McCaffery, J.M. Shaw, Dnm1p GTPase-mediated mitochondrial fission is a multi-step process requiring the novel integral membrane component Fis1p, J. Cell Biol. 151 (2000) 367–380.
[24] O.C. Loson, Z. Song, H. Chen, D.C. Chan, Fis1, Mff, MiD49, and MiD51 mediate Drp1 recruitment in mitochondrial fission, Mol. Biol. Cell 24 (2013) 659–667.
[25] S.J. Marrink, H.J. Risselada, S. Yefimov, D.P. Tieleman, A.H. de Vries, The MARTINI force field: coarse grained model for biomolecular simulations, J. Phys. Chem. B 111 (2007) 7812–7824.
[26] H.I. Ingólfsson, C.A. Lopez, J.J. Uusitalo, D.H. de Jong, S.M. Gopal, X. Periole, S.J. Marrink, The power of coarse graining in biomolecular simulations, Wiley Interdiscip. Rev.: Comput. Mol. Sci. 4 (2014) 225–248.
[27] T.A. Wassenaar, H.I. Ingolfsson, R.A. Bockmann, D.P. Tieleman, S.J. Marrink, Computational lipidomics with insane: a versatile tool for generating custom membranes for molecular simulations, J. Chem. Theory Comput. 11 (2015) 2144–2155.
[28] S.J. Marrink, A.H. de Vries, A.E. Mark, Coarse grained model for semiquantitative lipid simulations, J. Phys. Chem. B 108 (2004) 750–760.
[29] C.A. Lopez, Z. Sovova, F.J. van Eerden, A.H. de Vries, S.J. Marrink, Martini force field parameters for glycolipids, J. Chem. Theory Comput. 9 (2013) 1694–1708.
[30] H.I. Ingolfsson, M.N. Melo, F.J. van Eerden, C. Arnarez, C.A. Lopez, T.A. Wassenaar, X. Periole, A.H. de Vries, D.P. Tieleman, S.J. Marrink, Lipid organization of the plasma membrane, J. Am. Chem. Soc. 136 (2014) 14554–14559.
[31] M. Dahlberg, A. Maliniak, Mechanical properties of coarse-grained bilayers formed by Cardiolipin and Zwitterionic lipids, J. Chem. Theory Comput. 6 (2010) 1638–1649.
[32] D.H. de Jong, G. Singh, W.F.D. Bennett, C. Arnarez, T.A. Wassenaar, L.V. Schafer, X. Periole, D.P. Tieleman, S.J. Marrink, Improved parameters for the Martini coarse-

grained protein force field, J. Chem. Theory Comput. 9 (2013) 687–697.
[33] M.N. Melo, R. Ferre, M.A.R.B. Castanho, OPINION antimicrobial peptides: linking partition, activity and high membrane-bound concentrations, Nat. Rev. Microbiol. 7 (2009) 245–250.
[34] B. Hess, C. Kutzner, D. van der Spoel, E. Lindahl, GROMACS 4: algorithms for highly efficient, load-balanced, and scalable molecular simulation, J. Chem. Theory Comput. 4 (2008) 435–447.
[35] H.J.C. Berendsen, J.P.M. Postma, W.F. Vangunsteren, A. Dinola, J.R. Haak, Molecular-dynamics with coupling to an external bath, J. Chem. Phys. 81 (1984) 3684–3690.
[36] D.H. de Jong, S. Baoukina, H.I. Ingólfsson, S.J. Marrink, Martini straight: boosting performance using a shorter cutoff and GPUs, Comput. Phys. Commun. 199 (2016) 1–7.
[37] R. Fraser, J. Glasgow, A demonstration of clustering in protein contact maps for alpha helix pairs, International Conference on Adaptive and Natural Computing Algorithms, Springer, 2007, pp. 758–766.
[38] R.A. Jarvis, E.A. Patrick, Clustering using a similarity measure based on shared near neighbors, IEEE T. Comput. C-22 (1973) 1025–1034.
[39] R.J. Gowers, M. Linke, J. Barnoud, T.J.E. Reddy, M.N. Melo, S.L. Seyler, D.L. Dotson, J. Domanski, S. Buchoux, I.M. Kenney, MDAnalysis: a Python package for the rapid analysis of molecular dynamics simulations, in: S. Benthall, S. Rostrup (Eds.), Proceedings of the 15th Python in Science Conference, SciPy, Austin, TX, 2016, pp. 102–109.
[40] N. Michaud-Agrawal, E.J. Denning, T.B. Woolf, O. Beckstein, MDAnalysis: a toolkit for the analysis of molecular dynamics simulations, J. Comput. Chem. 32 (2011) 2319–2327.
[41] R. Volkmer, Synthesis and application of peptide arrays: quo vadis SPOT technology, Chem. Bio. Chem. 10 (2009) 1431–1442.
[42] K.N. Faber, G.J. Haan, R.J. Baerends, A.M. Kram, M. Veenhuis, Normal peroxisome development from vesicles induced by truncated Hansenula polymorpha Pex3p, J. Biol. Chem. 277 (2002) 11026–11033.
[43] C. Williams, L. Opalinski, C. Landgraf, J. Costello, M. Schrader, A.M. Krikken, K. Knoops, A.M. Kram, R. Volkmer, I.J. van der Klei, The membrane remodeling protein Pex11p activates the GTPase Dnm1p during peroxisomal fission, Proc. Natl. Acad. Sci. U. S. A. 112 (2015) 6377–6382.
[44] J.P. van Dijken, R. Otto, W. Harder, Growth of Hansenula polymorpha in a methanol-limited chemostat. Physiological responses due to the involvement of methanol oxidase as a key enzyme in methanol metabolism, Arch. Microbiol. 111 (1976) 137–144.
[45] R.J. Baerends, K.N. Faber, A.M. Kram, J.A. Kiel, I.J. van der Klei, M. Veenhuis, A stretch of positively charged amino acids at the N terminus of Hansenula polymorpha Pex3p is involved in incorporation of the protein into the peroxisomal membrane, J. Biol. Chem. 275 (2000) 9986–9995.
[46] A.A. Polyansky, R. Ramaswamy, P.E. Volynsky, I.F. Sbalzarini, S.J. Marrink, R.G. Efremov, Antimicrobial peptides induce growth of Phosphatidylglycerol domains in a model bacterial membrane, J. Phys. Chem. Lett. 1 (2010) 3108–3111.
[47] M.H. Fakieh, P.J. Drake, J. Lacey, J.M. Munck, A.M. Motley, E.H. Hettema, Intra-ER sorting of the peroxisomal membrane protein Pex3 relies on its luminal domain, Biol. Open 2 (2013) 829–837.
[48] A.A. Toro, C.A. Araya, G.J. Cordova, C.A. Arredondo, H.G. Cardenas, R.E. Moreno, A. Venegas, C.S. Koenig, J. Cancino, A. Gonzalez, M.J. Santos, Pex3p-dependent peroxisomal biogenesis initiates in the endoplasmic reticulum of human fibroblasts, J. Cell. Biochem. 107 (2009) 1083–1096.
[49] M. Veenhuis, I.J. van der Klei, A critical reflection on the principles of peroxisome formation in yeast, Front. Physiol. 5 (2014) 110.
[50] Y. Shibata, J. Hu, M.M. Kozlov, T.A. Rapoport, Mechanisms shaping the membranes of cellular organelles, Annu. Rev. Cell Dev. Biol. 25 (2009) 329–354.
[51] J.A. Kiel, I.J. van der Klei, M.A. van den Berg, R.A. Bovenberg, M. Veenhuis, Overproduction of a single protein, Pc-Pex11p, results in 2-fold enhanced penicillin production by Penicillium chrysogenum, Fungal Genet. Biol. 42 (2005) 154–164.
[52] T. Orth, S. Reumann, X. Zhang, J. Fan, D. Wenzel, S. Quan, J. Hu, The PEROXIN11 protein family controls peroxisome proliferation in Arabidopsis, Plant Cell 19 (2007) 333–350.
[53] S. Thoms, R. Erdmann, Dynamin-related proteins and Pex11 proteins in peroxisome division and proliferation, FEBS J. 272 (2005) 5169–5181.
[54] J. Koch, C. Brocard, Membrane elongation factors in organelle maintenance: the case of peroxisome proliferation, Biomol. Concepts 2 (2011) 353–364.
[55] M.S. Ebberink, J. Koster, G. Visser, F. Spronsen, I. Stolte-Dijkstra, G.P. Smit, J.M. Fock, S. Kemp, R.J. Wanders, H.R. Waterham, A novel defect of peroxisome division due to a homozygous non-sense mutation in the PEX11beta gene, J. Med. Genet. 49 (2012) 307–313.
[56] N.A. Bonekamp, S. Grille, M.J. Cardoso, M. Almeida, M. Aroso, S. Gomes, A.C. Magalhaes, D. Ribeiro, M. Islinger, M. Schrader, Self-interaction of human Pex11pbeta during peroxisomal growth and division, PLoS One 8 (2013) e53424.
[57] M.N. Cepinska, M. Veenhuis, I.J. van der Klei, S. Nagotu, Peroxisome fission is associated with reorganization of specific membrane proteins, Traffic 12 (2011) 925–937.
[58] H. Rottensteiner, K. Stein, E. Sonnenhol, R. Erdmann, Conserved function of pex11p and the novel pex25p and pex27p in peroxisome biogenesis, Mol. Biol. Cell 14 (2003) 4316–4328.
[59] Y.Y. Tam, J.C. Torres-Guzman, F.J. Vizeacoumar, J.J. Smith, M. Marelli, J.D. Aitchison, R.A. Rachubinski, Pex11-related proteins in peroxisome dynamics: a role for the novel peroxin Pex27p in controlling peroxisome size and number in Saccharomyces cerevisiae, Mol. Biol. Cell 14 (2003) 4089–4102.
[60] T. Wriessnegger, G. Gubitz, E. Leitner, E. Ingolic, J. Cregg, B.J. de la Cruz, G. Daum, Lipid composition of peroxisomes from the yeast Pichia pastoris grown on different carbon sources, Biochim. Biophys. Acta 1771 (2007) 455–461.
[61] A. Imazaki, A. Tanaka, Y. Harimoto, M. Yamamoto, K. Akimitsu, P. Park, T. Tsuge, Contribution of peroxisomes to secondary metabolism and pathogenicity in the fungal plant pathogen Alternaria alternata, Eukaryot. Cell 9 (2010) 682–694.
[62] N.E. Braverman, A.B. Moser, Functions of plasmalogen lipids in health and disease, Biochim. Biophys. Acta 1822 (2012) 1442–1452.
[63] A. Kawalek, C. Jagadeesan, I.J. van der Klei, Impaired biosynthesis of the non-bilayer lipids phosphatidylethanolamine or cardiolipin does not affect peroxisome biogenesis and proliferation in Saccharomyces cerevisiae, Biochem. Biophys. Res. Commun. 480 (2016) 228–233.